Pathways of Lipid Vesicle Deposition on Solid Surfaces: A Combined QCM-D and AFM Study

Ralf Richter,* Anneke Mukhopadhyay,† and Alain Brisson*

*Laboratoire d'Imagerie Moléculaire et Nano-Bio-Technologie, Institut Europeen de Chimie et Biologie, Université Bordeaux 1, 33607 Pessac Cedex, France; and †Department of Biophysical Chemistry, Groningen Biomolecular Sciences and Biotechnology Institute, University of Groningen, Nijenborgh 4, 9747 AG Groningen, The Netherlands

ABSTRACT Supported lipid bilayers (SLBs) are popular models of cell membranes with potential biotechnological applications, yet the mechanism of SLB formation is only partially understood. In this study, the adsorption and subsequent conformational changes of sonicated unilamellar vesicles on silica supports were investigated by quartz crystal microbalance with dissipation monitoring and atomic force microscopy, using mixtures of zwitterionic, negatively charged, and positively charged lipids, both in the presence and in the absence of Ca^{2+} ions. Four different pathways of vesicle deposition could be distinguished. Depending on their charge, vesicles i), did not adsorb; ii), formed a stable vesicular layer; or iii), decomposed into an SLB after adsorption at high critical coverage or iv), at low coverage. Calcium was shown to enhance the tendency of SLB formation for negatively charged and zwitterionic vesicles. The role of vesicle-support, interbilayer, and intrabilayer interactions in the formation of SLBs is discussed.

INTRODUCTION

Supported lipid bilayers (SLBs[1]) are popular as model systems for cell membranes (Watts et al., 1984, 1986; Sackmann, 1996; Salafsky et al., 1996) and are promising for future applications in diagnostic devices and biomimetics (Cornell et al., 1997; Reviakine et al., 1998; Bieri et al., 1999; Kung et al., 2000). The creation of SLBs by the spreading of lipid vesicles on hydrophilic supports, pioneered by McConnell's group (Watts et al., 1984; McConnell et al., 1986), is attractive because of its simplicity and reproducibility. Considerable work, both experimental (Nollert et al., 1995; Rädler et al., 1995; Keller and Kasemo, 1998; Cremer and Boxer, 1999; Jass et al., 2000; Keller et al., 2000; Reviakine and Brisson, 2000; Johnson et al., 2002; Reimhult et al., 2002a,b) and theoretical (Lipowsky and Seifert, 1991; Seifert, 1997; Zhdanov et al., 2000; Zhdanov and Kasemo, 2001), has been devoted to understanding the driving forces involved in the adsorption of vesicles from solution and in the mechanisms of SLB formation.

Using techniques such as fluorescence microscopy (Nollert et al., 1995; Cremer and Boxer, 1999; Johnson et al., 2002), quartz crystal microbalance with dissipation monitoring (QCM-D) (Keller and Kasemo, 1998; Reimhult et al., 2002b), and atomic force microscopy (AFM) (Reviakine and Brisson, 2000), it has been established that vesicles made of PC lipids in the fluid phase form SLBs on silica, glass, or mica, whereas they do not rupture, forming stable supported vesicular layers (SVLs) on other surfaces such as titanium oxide or gold. Several studies have pointed to the influence of electrostatic interactions in general and the vesicle charge in particular on SLB formation (Nollert et al., 1995; Rädler et al., 1995; Cremer and Boxer, 1999). It is also well established that calcium can induce aggregation of negatively charged vesicles in solution (Wilschut et al., 1981; Marcelja, 1992) and influence the SLB formation of charged and neutral lipids (McLaughlin et al., 1978; Nollert et al., 1995; Reviakine and Brisson, 2000; Ekeroth et al., 2002) or the lipid domain distribution in SLBs (Reviakine et al., 2000). Although a clearer picture of the intermediates involved in SLB formation is emerging from recent studies, a detailed description of the respective contribution of the vesicle-support, intervesicle, and intravesicle interactions is still lacking.

We report here on a systematic study of the influence of vesicle charge and calcium-EDTA balance on the process of vesicle adsorption and SLB formation on silica. In this study, we combined a surface-sensitive method with high time resolution, QCM-D, and an imaging method with high spatial resolution, AFM, to investigate the behavior of vesicles with varying net charges, from positively charged pure dioleoyltrimethylammonium-propane (DOTAP) to mixtures of neutral dioleoylphosphatidylcholine (DOPC) and negatively charged dioleoylphospatidylserine (DOPS).

QCM-D, providing information about the mass and the conformational changes of adsorbed material, has been shown to be a useful tool to study the formation of SLBs (Keller and Kasemo, 1998; Keller et al., 2000; Reimhult et al., 2002a,b). In particular, the concept of an elevated critical vesicular coverage required to induce the decomposition of adsorbed vesicles into bilayer patches originated from QCM-D studies (Keller et al., 2000; Zhdanov et al., 2000).

AFM allows investigating the morphology of single vesicles and isolated bilayer patches (Jass et al., 2000;

Submitted February 12, 2003, and accepted for publication May 21, 2003.

Address reprint requests to Alain Brisson, E-mail: a.brisson@iecb-polytechnique.u-bordeaux.fr.

[1]The term SLB is used in this work, in contrast with the terms supported phospholipid bilayer (SPB) (Reviakine and Brisson, 2000) and supported planar bilayer (SPB) (Liebau et al., 2001), because it is a generalization valid for all types of lipids and surfaces of various roughness.

0006-3495/03/11/3035/13 $2.00

Pignataro et al., 2000; Reviakine and Brisson, 2000; Muresan and Lee, 2001) and following the formation of SLBs (Reviakine and Brisson, 2000), providing structural details of the SLB formation process.

Using this combined approach of QCM-D and AFM, several qualitatively different pathways of vesicle adsorption and SLB formation have been identified and characterized, and are reported here.

MATERIALS AND METHODS

Materials

DOPC, DOPS, and DOTAP were purchased from Avanti Polar Lipids (Alabaster, AL). Lyophilized cholera toxin B-subunit pentamer (B5), polyethylene glycol (PEG; average molecular weight 8 kDa), and other chemicals were purchased from Sigma (St. Louis, MO). Ultrapure water with a resistivity of 18.2 MΩ was used, prepared with a Maxima system (USF ELGA, Trappes, France). QCM-D sensor crystals (5 MHz), reactively sputter-coated with 50 nm silicon oxide, were purchased from Q-SENSE (Gothenburg, Sweden). Plates of (11 × 11) mm^2 of silicon wafer were provided by the Commissariat à l'Energie Atomique (Grenoble, France).

Buffer preparation

A buffer (buffer A) made of 150 mM NaCl, 2 mM NaN_3, and 10 mM HEPES, pH 7.4, was prepared in ultrapure water. EDTA or $CaCl_2$ was added to buffer A at 2 mM (final concentrations), respectively, as indicated in the text.

Vesicle preparation

Lipids were dissolved in chloroform, mixed in desired amounts, dried under a stream of nitrogen followed by drying in a vacuum desiccator overnight, resuspended at 1–2 mg/mL final concentration, and vortexed in EDTA buffer. Lipid mixtures were homogenized by five cycles of freeze-thawing and subsequent vortexing. Small unilamellar vesicles (SUVs) were obtained by sonication with a tip sonicator (Misonix, Farmingdale, NY) operated in a pulsed mode at 30% duty cycle for 30 min with refrigeration, followed by centrifugation in an Eppendorf centrifuge (10 min at 16,000 × g) to remove titanium particles. SUV suspensions were stored at 4°C under nitrogen and used within two weeks. Before use, vesicle suspensions were diluted to 0.1 mg/mL. Lipid concentrations were deduced from the mass of the lipids dissolved and, if applicable, by phosphorus content determination (Rouser et al., 1975) of the final lipid suspensions. Errors of <10% were obtained.

Protein preparation

B5 was resuspended in ultrapure water at 1 mg protein per mL. Before use, the solution was diluted to 10 μg/mL in the buffer used in the concerned measurement.

Substrate preparation

The QCM-D sensor crystals and silicon wafers were cleaned by two cycles of exposure to 2% sodium dodecyl sulfate solution for 15 min, rinsing with ultrapure water, blow-drying with nitrogen, and exposure to ultraviolet (UV)/ozone for 10 min. For UV/ozone treatment, the substrates were placed in the vicinity of a mercury grid lamp (BHK, Claremont, CA), mounted into a home-built chamber and driven by a suitable power source (BHK). Ozone is produced from the oxygen present in ambient air by the emitted UV light of wavelength 185 nm. By this treatment, the surface is cleaned from traces of organic contaminants (Vig, 1987) and rendered hydrophilic (Keller and Kasemo, 1998). In addition, the treatment enforces the formation of a thin layer of silica on the silicon wafer (Vig, 1987). The chemical nature of the surface of the silica wafers is thus expected to be similar to the silica coat on the QCM-D sensor crystals. Cleaned substrates were stored in air. Before use, they were re-exposed to UV/ozone for 10 min.

Quartz crystal microbalance with dissipation monitoring

QCM-D measurements were performed with the Q-SENSE D300 system equipped with a QAFC 301 axial flow chamber (Q-SENSE), as described in detail elsewhere (Rodahl et al., 1995). Upon interaction of (soft) matter with the surface of a sensor crystal, changes in the resonance frequency, f, related to attached mass (including coupled water), and in the dissipation, D, related to frictional (viscous) losses in the adlayer are measured with a time resolution of better than 1 s.

Measurements were performed in exchange mode, i.e., a volume of ~0.5 mL of temperature-stabilized and degassed sample liquid was delivered to the chamber containing the sensor crystal (internal volume, 50 μL) to ensure a complete exchange of the liquid. Signal distortion (peaks of $|\Delta f| < 5$ Hz and $|\Delta D| < 0.6 \cdot 10^{-6}$ are commonly observed) upon flushing is limited to a few seconds. In this way, processes of adsorption and surface adlayer changes can be followed in situ while subsequently exposing different solutions to the surface. Measurement data for f and D were acquired at several harmonics (15, 25, and 35 MHz) simultaneously. All measurements were performed at a temperature of 24–25°C, to within 0.05 K.

If not stated otherwise, changes in dissipation and normalized frequency ($\Delta f_{norm} = f_n/n$, with n being the overtone number) of the third overtone (n = 3, i.e., 15 MHz) are presented here. Adsorbed masses, Δm, are deduced according to the Sauerbrey equation, $\Delta f_{norm} = -\Delta m/C$, with C = 17.7 ng cm^{-2} Hz^{-1}, valid for thin, rigid films coupled without friction to the sensor surface. The equation has been demonstrated to be valid for lipid bilayers on surfaces (Keller and Kasemo, 1998) and to slightly underestimate the mass of adsorbed, nonruptured SUVs (error in the order of 5% (Reimhult et al., 2002b)).

Atomic force microscopy

AFM measurements were performed in liquid using a Nanoscope VI-MultiMode (Veeco, Dourdan, France), equipped with a J-scanner (120 μm). The tapping-mode fluid cell was washed by sonication in successive baths of ethanol and ultrapure water, followed by extensive rinsing in ethanol and blow-drying in a stream of nitrogen.

Oxide-sharpened silicon nitride cantilevers with a nominal spring constant of 0.06 N/m (Digital Instruments, Santa Barbara, CA) were exposed to UV/ozone for 10 min, immersed in a 3% PEG solution for 1 h and extensively rinsed with buffer before mounting in the AFM cell.

Silicon wafers were attached to Teflon-coated metal disks (BYTAC, Norton, OH), using double-sided tape (TESA, Hamburg, Germany) and covered with buffer. Vesicle solutions were added in desired concentrations, incubated for desired times, extensively rinsed with buffer, and installed on the AFM scanner. The AFM was equilibrated for 30 min before imaging. For further incubation of vesicles, the AFM head was unmounted and subsequently remounted without disrupting the liquid film present on the wafer.

Images were acquired in tapping mode at a scanning rate of 1 Hz and a scan angle of 90°. A resonance frequency ~7 kHz was chosen with low free amplitude (0.3–0.4 V) and low load upon scanning. Images were flattened and plane-fitted except when otherwise stated.

Lipid structures such as surface-bound vesicles are known to be easily modified by interactions with the AFM tip (Jass et al., 2000; Reviakine and Brisson, 2000; Richter and Brisson, 2003). Images were recorded in tapping mode with PEG-modified tips as this setup was observed to show the smallest tip-sample interactions. The substrate of choice for the AFM studies

was the silica wafer because its flatness allows easy detection of objects in contrast to the rough QCM-D crystal surface (Richter and Brisson, 2003).

RESULTS

Pathways of vesicle deposition by QCM-D

Three basic types of QCM-D responses were obtained, depending on the lipid mixture used and the calcium-EDTA balance (Fig. 1).

Formation of a supported vesicular layer

Upon adsorption of SUVs made of DOPC and DOPS (molar ratio 1:1) in the presence of EDTA, the frequency decreases monotonically and equilibrates slowly at a level of $\Delta f_{fin} = -54 \pm 4$ Hz (Fig. 1 *A*). The dissipation increases and equilibrates at an elevated level of $\Delta D_{fin} = 2.9 \pm 0.3 \cdot 10^{-6}$. These Δf_{fin} and ΔD_{fin} values are representative of the formation of a flexible layer of vesicles, as reported previously by Keller and Kasemo (1998) for egg yolk phosphatidylcholine (egg-PC) on gold. f and D remain stable upon rinsing with buffer, indicating that the vesicles are adsorbed in a stable manner at timescales investigated here.

Formation of a continuous SLB: case 1

The QCM-D response observed when adsorbing SUVs made of DOPC/DOPS (molar ratio 4:1) in the presence of EDTA shows a two-phase process (Fig. 1 *B*). The initial phase is similar to the case described above. However, after reaching extremes, $\Delta f_{min} = -58$ Hz and $\Delta D_{max} = 2.4 \cdot 10^{-6}$, a second phase is observed, which is characterized by an increase of the frequency and a decrease of the dissipation, equilibrating at levels of $\Delta f_{fin} = -24.5$ Hz and $\Delta D_{fin} = 0.1 \cdot 10^{-6}$, respectively. This behavior is similar to a response previously reported for egg-PC on silica (Keller and Kasemo, 1998; Keller et al., 2000), which was interpreted as follows: the first phase reflects the adsorption of a vesicular layer of elevated coverage, Δf_{min} being a measure for the vesicular coverage; the second phase corresponds to the formation of a continuous SLB. The value of $\Delta f_{fin} = -24.5$ Hz corresponds to an adsorbed mass of 434 ng/cm^2. Taking into account the average molecular lipid weight and the lipid molecular area, this value supports the view of a continuous hydrated SLB (Keller and Kasemo, 1998).

If rinsing with buffer is performed before the expected minimum frequency, the Δf and ΔD signals remain constant (data not shown). In contrast, rinsing after the minimum frequency results in further increase of f and decrease of D, indicating ongoing vesicle decomposition (Keller et al., 2000) (data not shown).

To verify whether lipids covered the entire silica surface, the B5 protein was used as a reporter of accessible silica surface. Control experiments showed indeed that B5 is adsorbing onto silica at high coverage ($\Delta f = -15$ Hz, data not shown) as well as to mica but not to DOPC/DOPS SLBs (Reviakine and Brisson, 2000). No binding of B5 was detectable after formation of a DOPC/DOPS SLB (data not shown), indicating that the SLB was continuous.

Formation of a continuous SLB: case 2

Fig. 1 *C* shows the adsorption behavior of pure DOTAP SUVs in EDTA. Upon adsorption, the frequency decreases monotonically, reaching an equilibrium level of $\Delta f_{fin} = -20.5$ Hz. The dissipation shows a peak ($\Delta D_{max} = 0.6 \cdot 10^{-6}$) soon after the onset of adsorption (at $\Delta f = -12$ Hz) before equilibrating at a level of $\Delta D_{fin} = 0.2 \cdot 10^{-6}$. Further addition of B5 resulted in low amounts of adsorption ($|\Delta f| \leq 0.5$ Hz, data not shown), indicating that an SLB covered most of the surface, but local defects estimated to represent <5% of the surface subsisted.

For this response, not reported in the literature before, we propose the following interpretation: i), an SLB is formed, covering most of the surface, and ii), the onset of bilayer formation occurs at low surface coverage, in opposition to case 1, indicating that either adsorbed SUVs rupture spontaneously, or that only a few contacts between adsorbed

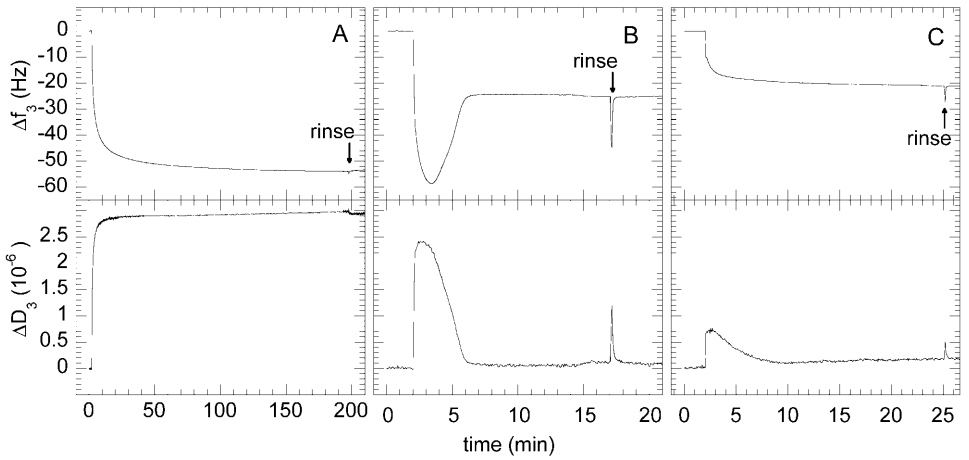

FIGURE 1 QCM-D responses for the deposition of different lipid mixtures on SiO_2 in the presence of 2 mM EDTA. Changes in frequency and dissipation at 15 MHz (*upper* and *lower panels*, respectively). (*A*) DOPC/DOPS (molar ratio increase 1:1), example of formation of an SVL. (*B*) DOPC/DOPS (4:1), example of SLB formation (case 1) triggered at an elevated critical vesicular coverage. (*C*) DOTAP, example of SLB formation (case 2) triggered at low vesicular coverage. Lipid exposure starts at 2 min; rinses with EDTA-containing buffer (*arrows*).

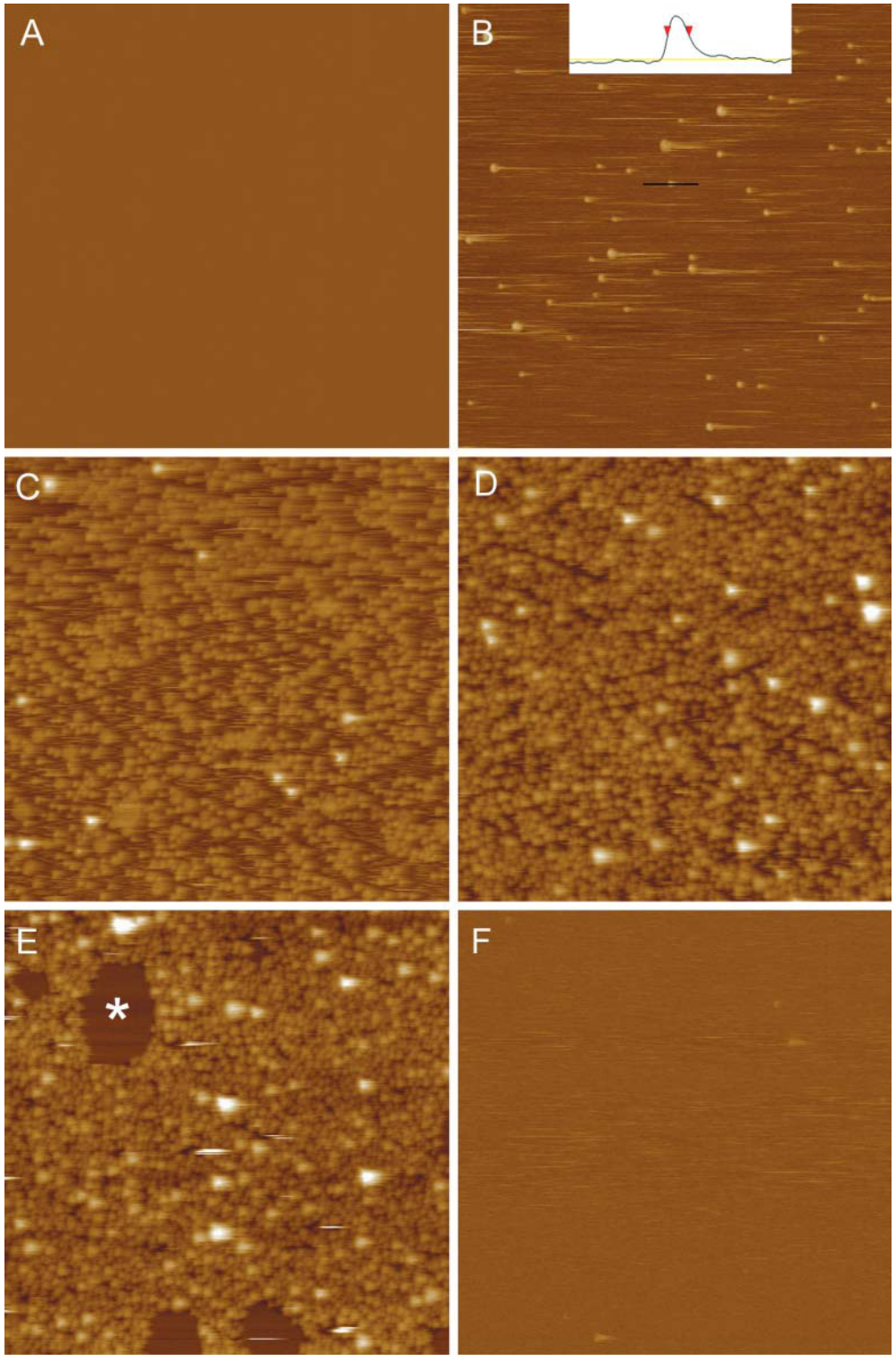

FIGURE 2 ''Snapshots'' of the SLB-formation process for DOPC/DOPS (4:1) on a silica wafer by AFM. The support was subsequently exposed to lipid concentrations (exposure time) of (*A*) 0 μg/mL (0 min), (*B*) 1 μg/mL (5 min), (*C*) 5 μg/mL (3 min) + 8 μg/mL (8 min), (*D*) 7 μg/mL (10 min) + 10 μg/mL (15 min), (*E*) 16 μg/mL (10 min), and (*F*) 25 μg/mL (10 min) before rinsing with buffer and imaging. To minimize the effect of tip artifacts, a new spot on the wafer was used for each AFM image. Image size (*z*-scale), 2 μm (50 nm). (*B*, *inset*) Cross section showing a circular object of 12-nm height and 25-nm width identified as an adsorbed vesicle. Tails along the scan direction are believed to be due to a combination of weak tip-sample interaction and low gains chosen for image acquisition. (*B–E*) Vesicular coverage increases. (*E*) At high coverage, bilayer patches (*asterisk*) are observed.

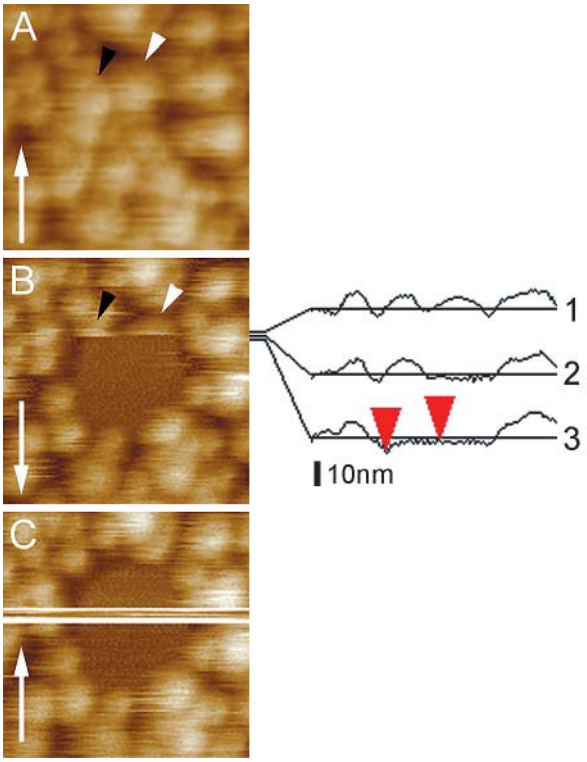

FIGURE 3 AFM images of an event of vesicle rupture and bilayer patch formation. The images were subsequently recorded on the same spot at a stage of bilayer formation of DOPC/DOPS (4:1) corresponding to Fig. 2 *D*. The slow scan direction is indicated (*arrows*). Fast scan direction from right to left. Image size (*z*-scale), 250 nm (40 nm). (*A*) First image, all vesicles are intact. (*B*) Second image, two vesicle segments are resolved (*arrowheads*) followed by a bilayer domain, indicating the rupture of vesicles. Cross sections of subsequent scan lines (*right*), the right vesicle (*white arrowhead*) is transformed into a bilayer patch induced by the AFM tip. The left vesicle next to it (*black arrowhead*) remains intact at scan line 2. At scan line 3, the left vesicle is ruptured, likely induced by the ''active edge'' of the bilayer patch originating from the vesicle ruptured first. The height between the red markers, 4.1 nm, corresponds to the thickness of a bilayer. (*C*) Third image, the rupture of single vesicles induced the transformation of adjacent vesicles into a stable bilayer patch. A small gap (a few nanometers) separates the patch edges from neighboring intact vesicles. A part of the image is distorted because the tip was accidentally retracted from the surface.

vesicles are necessary to induce the formation of bilayer patches.

Vesicle deposition and bilayer formation by AFM

Whereas QCM-D allows a global characterization of the vesicle deposition process with high temporal resolution, AFM was employed to provide information on the local organization of surface-bound lipid material. We focused on the two pathways that lead to SLB formation. ''Snapshots'' of the process of vesicle adsorption and SLB formation were recorded after adding SUV solutions of increasing concentration in a stepwise fashion. For practical reasons, calcium-containing buffer was used for these experiments.

Formation of a continuous SLB: case 1

A series of images obtained for vesicles of DOPC/DOPS (4:1) is shown in Fig. 2. Adsorbed SUVs are resolved as round objects with a minimum diameter of 20–25 nm and a minimum height of 12 nm, as previously described (Reviakine and Brisson, 2000). The vesicular coverage increased (Fig. 2, *B–D*) with increasing vesicle exposure. At an elevated coverage, flat patches appeared (*asterisk* in Fig. 2 *E*) and were determined to be supported bilayers (see below) that eventually formed a continuous defect-free bilayer (Fig. 2 *F*). The imaged lipid structures were stable and no lateral diffusion could be detected over the timescale of 1 h. Bilayer patches show predominantly convex but noncircular shapes. The size distribution of surface-bound vesicles did not change with increasing surface coverage, as evaluated by the eye.

Occasionally, the AFM tip was observed to induce the rupture of a vesicle (Fig. 3), which allowed us to access details of the process of SLB formation. As the vesicle decomposition is fast compared to the scan speed of the AFM, only a segment of the originally intact vesicle (*white arrowhead* in Fig. 3, *A* and *B*) was observed, whereas the rest was transformed into a bilayer (Jass et al., 2000). The rupture of a single vesicle induced the transformation of neighboring adsorbed vesicles into a bilayer patch (Fig. 3 *B*). The bilayer nature of the resulting patches is deduced from their homogeneous flatness and their height of ~4 nm. Bilayer patches corresponded in size to the merging of 5–50 immobilized vesicles, as determined by counting of the vesicles present before and after patch formation. Note that a small gap (a few nanometers) separates the patch edges from neighboring unruptured vesicles. A detailed analysis of the tip-induced vesicle decomposition event shown in Fig. 3 *B* provides further information on the process of rupture propagation. Considering that one vesicle (*white arrowhead*) is ruptured at the scan line shown in cross section 2, a second vesicle next to it (*black arrowhead*) remains intact at this scan line, whereas it is ruptured at the subsequent scan line (cross section 3). Similar images were found repeatedly, and, because tip-induced rupture events are extremely rare, we must conclude that the rupture of the second vesicle (*black arrowhead*) was induced by the rupture of the first vesicle (*white arrowhead*) within ~1 s, most likely due to the ''active edge'' effect. The fact that no larger vesicle could be detected by AFM in the vicinity of ruptured vesicles suggests that fusion between vesicles does not take place in this system.

Formation of a continuous SLB: case 2

A similar series of AFM images was recorded to follow the process of SLB formation with SUVs of DOTAP (Fig. 4). At low lipid coverage, flat patches with a height of ~4 nm are observed, as expected for bilayer patches. The smallest

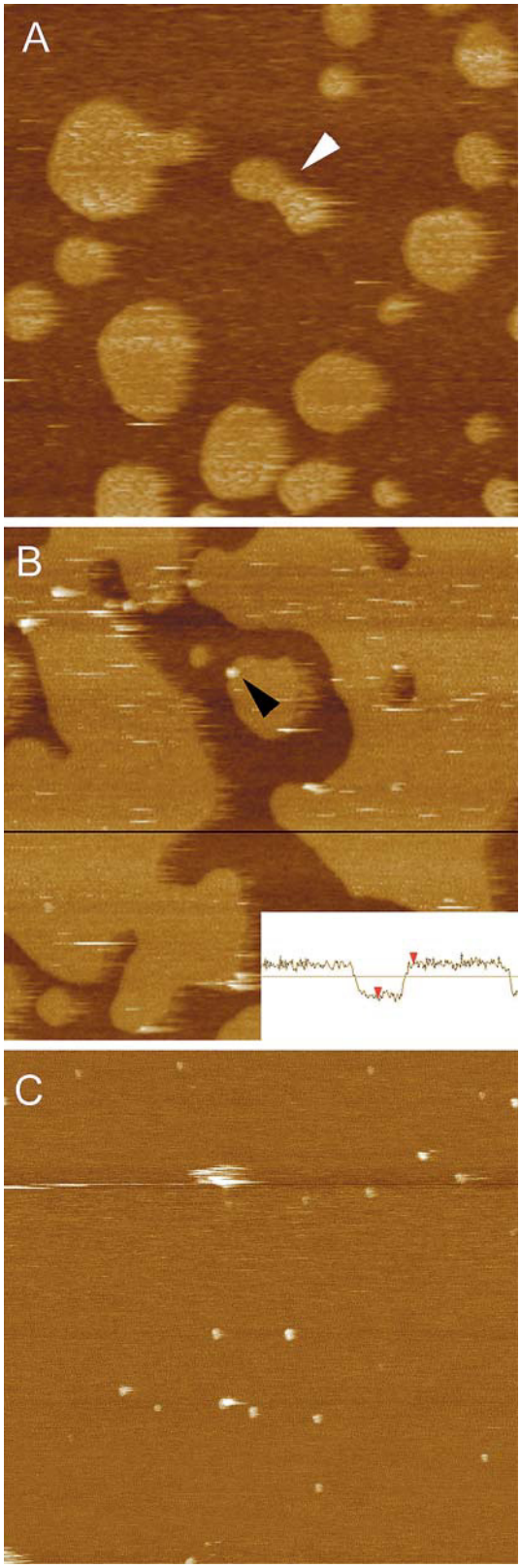

FIGURE 4 ''Snapshots'' of the SLB-formation process for DOTAP on a silica wafer. The support was subsequently exposed to lipid concentrations (exposure time) of (*A*) 1 μg/mL (4 min) + 2 μg/mL (20 min), (*B*) 5 μg/mL (6 min) + 8 μg/mL (20 min) + 25 μg/mL (20 min), and (*C*) 130 μg/mL (30 min) before rinsing with buffer and imaging. To minimize the effect of tip artifacts, a new spot on the wafer was used for each AFM image. Image size (*z*-scale), 1 μm (20 nm). (*B*) Flat domains with a height of ~4 nm (*inset*, height between red markers, 4.1 nm) identified as bilayer patches. (*A*) The dumbbell-like shape of a patch (*white arrowhead*) appears to be the result of two decomposed vesicles. With increasing coverage, domains merge (*A* and *B*) and eventually form a continuous bilayer (*C*). Elevated objects of ~20 nm diameter, initially observed predominantly at (*B*) the edges of growing patches (*black arrowhead*), remain upon completion of the SLB formation and are suggested to result from contaminations in the DOTAP solution.

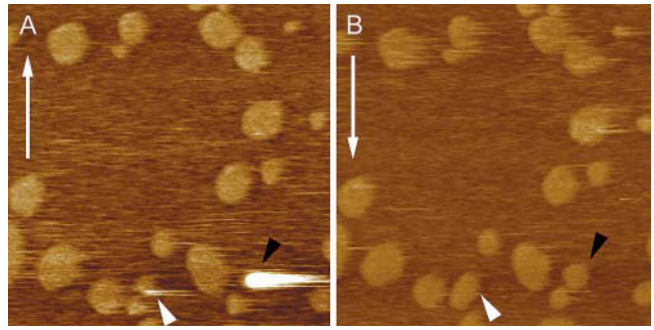

FIGURE 5 AFM images subsequently recorded on the same spot at an early stage of bilayer formation of DOTAP. The slow scan direction is indicated (*arrows*). Fast scan direction from left to right. Image size (*z*-scale), 1 μm (20 nm). (*A*) First image, vesicle segments (*white arrowhead*) indicate rupture induced by the AFM tip. Rarely, entire vesicles (*black arrowhead*) can be observed. (*B*) Second image, all vesicles have transformed into bilayer patches (*arrowheads*).

patches have a diameter of 40 nm, as expected for single ruptured SUVs. The diameter of the patches ranges from 40 nm to 250 nm, corresponding to approximate vesicle sizes of 25–125 nm. The size distribution is thus considerably larger as compared with DOPC/DOPS (4:1). Note the dumbbell-like shape of some bilayer patches (*arrowhead* in Fig. 4 *A*), which appears to be the result of two or more decomposed vesicles. The patch morphology was stable upon repeated imaging.

Bilayer patches coalesce with increasing vesicle exposure (Fig. 4, *A* and *B*) and finally form a film that entirely covers the surface (Fig. 4 *C*). A number of elevated objects of ~20 nm diameter, observed initially predominantly at the edges of growing patches (*arrowhead* in Fig. 4 *C*), remain when the SLB formation is complete. They do not diffuse and are stable upon enhanced forces exerted by the AFM tip. The fact that they are immobilized together with the lipids suggests that these defects result from contaminations in the DOTAP solution.

Occasionally, the presence of immobilized unruptured vesicles was detected at low lipid coverage (Fig. 5). Most of these vesicles could be visualized only in part (*white arrowheads* in Fig. 5 *A*)—despite exceptions (*black arrowhead* in Fig. 5 *A*)—and were transformed into a bilayer patch during the first scan, indicating a high susceptibility to interactions with the AFM tip. The fact that the AFM signal

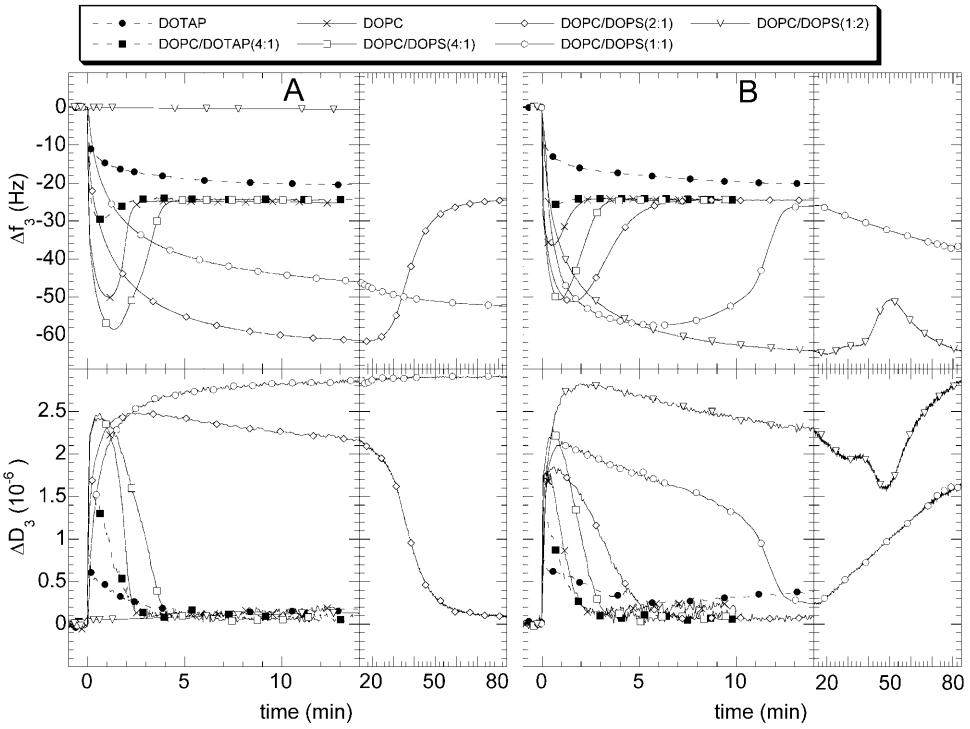

FIGURE 6 QCM-D response for the deposition of various lipid mixtures, indicated in the upper inset, on SiO_2 in the presence of 2 mM EDTA (*A*) and 2 mM $CaCl_2$ (*B*). Changes in frequency (*upper panel*) and dissipation (*lower panel*) are given for the third overtone (15 MHz). The timescale is split into two parts to allow representation of the complete deposition process for DOPC/DOPS (molar ratio 2:1 (*A*), 1:1 (*A* and *B*), and 1:2 (*B*)).

is highly sensitive to the presence of vesicle remnants and that most bilayer patches are devoid of any associated remnants indicates that the DOTAP vesicles rupture spontaneously before interaction with the tip.

Charge dependence of vesicle adsorption and SLB formation

The three pathways of vesicle deposition presented above reveal the influence of the charge of SUVs on the process of vesicle deposition and SLB formation. The effects of lipid composition and calcium-EDTA balance were then investigated in a systematic manner by QCM-D. The deposition of SUVs made of the lipid mixtures DOTAP, DOPC/DOTAP (molar ratio, 4:1), DOPC, and DOPC/DOPS (4:1, 2:1, 1:1, and 1:2) was followed both in the presence of the calcium chelator EDTA (Fig. 6 *A*) and in the presence of Ca^{2+} ions (Fig. 6 *B*). The results are summarized in Table 1.

In the presence of EDTA, SLB formation of case 1 was observed for pure DOPC and at low positive (DOPC/DOTAP (4:1)) and negative (DOPC/DOPS (4:1, 2:1)) vesicle charges. At high negative charge (DOPC/DOPS (1:2)), no adsorption was measurable over the time range of 2 h ($|\Delta f| < 1$ Hz, data not shown). This situation is herewith referred to as the fourth pathway.

In the presence of Ca^{2+} ions, bilayer formation was initiated for all lipid mixtures investigated (Fig. 6 *B*). Pure DOTAP showed SLB formation of case 2. For pure DOPC and mixtures with low content of charged lipids (DOPC/DOTAP (4:1)) and DOPC/DOPS (4:1, 2:1), the SLB was complete (case 1) and stable. At intermediate (DOPC/DOPS (1:1)) and high (DOPC/DOPS (1:2)) negative lipid charge, an additional process set in during SLB formation that we refer to as restructuration and describe hereafter.

In the case of bilayer formation of case 1, $|\Delta f_{min}|$ showed pronounced charge dependence (Fig. 7 *A*). $|\Delta f_{min}|$ increased when scanning from positive charge to negative charge, both with Ca^{2+} ions and with EDTA. At a given charge content, $|\Delta f_{min}|$ was smaller in the presence of Ca^{2+} ions. A final frequency shift of $\Delta f_{fin} = -24.5 \pm 0.5$ Hz ($n = 13$) was measured for all lipid mixtures studied, except for DOTAP and for conditions leading to restructuration (see below). The low value obtained with DOTAP ($\Delta f_{fin} = -20.5 \pm 0.5$ Hz, $n = 4$) could in part be attributed to an incomplete coverage of the silica surface, as described above. In addition, differences in molecular weight, surface area occupied per lipid molecule, or hydration of the lipid headgroup between DOTAP and either DOPC or DOPS are likely to explain remaining deviations.

Kinetics of initial vesicle adsorption and SLB formation

In terms of kinetics, two phases need to be distinguished: i), the initial adsorption of vesicles, and ii), vesicle adsorption and conformational changes at elevated surface coverage.

Kinetics of the initial adsorption of vesicles

In the presence of EDTA, lipid mixtures with positive (DOTAP, DOPC/DOTAP (4:1)), neutral (DOPC), and low

TABLE 1 Parameters measured by QCM-D for the deposition of vesicles with varying lipid composition

Lipid ratio			[Ca]	Δf_{min}	m_{max}	ΔD_{max}	Δf_{fin}	m_{fin}	ΔD_{fin}	t_{SLB}	Vesicle deposition
DOTAP	DOPC	DOPS	(mM)	(Hz)	(ng/cm^2)	(10^{-6})	(Hz)	(ng/cm^2)	(10^{-6})	(min)	pathway
1	-	-	0	-	-	0.8	−20.5	363	0.2	10	SLB (I)
1	4	-	0	−32	566	1.5	−24.5	434	0.1	3	SLB (II)
-	1	-	0	−52	920	2.4	−25	443	0.15	3	SLB (II)
-	4	1	0	−60	1062	2.4	−24.5	434	0.1	4.5	SLB (II)
-	2	1	0	−62	1097	2.5	−24.5	434	0.1	80	SLB (II)
-	1	1	0	−54	956	2.9	-	-	-	-	SVL
-	1	2	0	0	0	0	-	-	-	-	No adsorption
1	-	-	2	-	-	0.75	−20.5	363	0.35	11	SLB (I)
1	4	-	2	−26	460	1.4	−24.5	434	0.1	2	SLB (II)
-	1	-	2	−35	620	1.8	−24.5	434	0.2	2.6	SLB (II)
-	4	1	2	−51	903	2.3	−24.5	434	0.1	3.3	SLB (II)
-	2	1	2	−53	938	1.8	−24.5	434	0.1	8	SLB (II)
-	1	1	2	−59	1044	2.1	-	-	-	17*	SLB (II), restructuration
-	1	2	2	−65	1151	2.8	-	-	-	57*	SLB (II), restructuration

*Extrapolated estimates.

negative (DOPC/DOPS (4:1)) charge show similar initial adsorption rates. Kinetics slow down with increasing negative charge (DOPC/DOPS (2:1, 1:1)), and no adsorption is detected with DOPC/DOPS (1:2). A similar trend is observed in the presence of calcium, though the slowdown of kinetics is shifted toward higher negative-charge content. Considering the experimental setup chosen (essentially standing liquid), it is likely that adsorption is transport-controlled (Adamczyk et al., 1994) at net-positive, net-neutral, or low net-negative vesicle charge. The decreased rate of initial adsorption observed at high negative vesicle charge indicates that the adsorption becomes limited by an energy barrier. The barrier increases with increasing negative lipid charge and decreases in the presence of calcium.

Kinetics of SLB formation

Both in the presence of EDTA and in the presence of calcium, the time, t_{SLB}, needed to form an SLB is smallest for DOPC and DOPC/DOTAP(1:4) and increases with increasing negative vesicle charge (Fig. 7 *B*). For DOPC- or DOPS-containing mixtures, bilayer formation is faster in calcium than in EDTA. For high positive lipid charge (pure DOTAP), note the extended time with slow adsorption rate before equilibration (Fig. 6).

Reproducibility

In the initial stage of investigations related to this study, it turned out that the preparation of both surface and SUVs could critically influence the process of vesicle deposition. In particular, the tendency to form SLBs and the quality of formed bilayers as well as the onset and extent of restructuration (see below) varied considerably. Rigorously following the above-indicated preparation protocol, however, enabled us to obtain reproducible results. Variations indicated as error bars above are derived from two to three measurements performed with the same SUV solutions of varied age (some hours to two weeks).

Restructuration

An additional response, not reported in the literature before, was observed for SUVs with intermediate and high negative lipid charge (DOPC/DOPS (1:1, 1:2)) in the presence of Ca^{2+} ions. During SLB formation, the increase in frequency and the decrease in dissipation were followed by a slow decrease/increase in f and D, respectively. For DOPC/DOPS (1:2), this process sets in early, whereas for DOPC/DOPS (1:1) (Fig. 8, referred to hereafter) the onset is near the end of SLB formation. The dissipation change, corresponding with $\Delta D = 1.3 \cdot 10^{-6}$ per hour of this ongoing process, is high with respect to the frequency change, $\Delta f = -10$ Hz per hour, indicating the presence of lipid material deposited in a flexible state. The surface adlayer remained essentially stable upon rinsing with a calcium-containing buffer (see *arrow 1* in Fig. 8), though the dissipation continued to increase. In contrast, rinsing with EDTA (*arrow 2* in Fig. 8) had a striking effect. An instantaneous increase in dissipation by more than $1 \cdot 10^{-6}$ was followed by a quick increase/decrease in f and D, respectively. Further rinsing with calcium-containing buffer (*arrow 3* in Fig. 8) resulted in final values for frequency, $\Delta f_{fin} = -24$ Hz, and dissipation, $\Delta D_{fin} = 0.2 \cdot 10^{-6}$, which are characteristic of a complete SLB. The formed bilayer was stable upon re-exposure to calcium-containing buffer or lipids (data not shown).

To better understand this process, lipids present in solution were washed away shortly after the maximum/minimum dissipation and frequency, respectively (*dashed curves* in Fig. 8). An initial increase in f and decrease in D were observed, which is believed to reflect ongoing vesicle

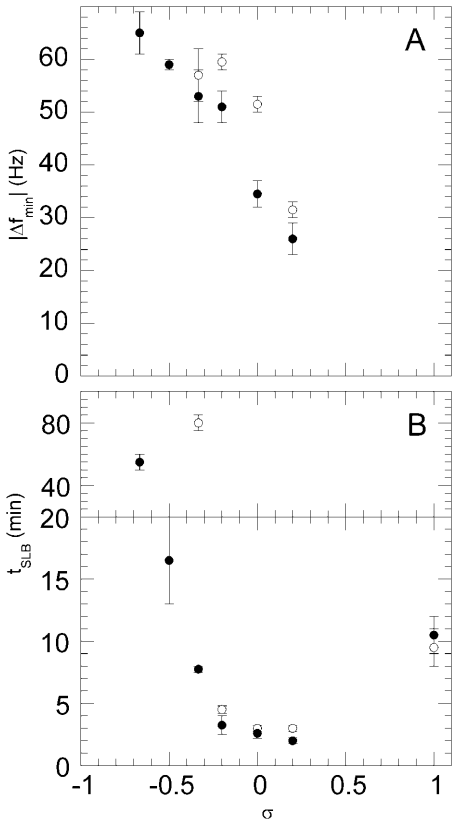

FIGURE 7 (*A*) Relationship between the local minimum frequency, $|\Delta f_{min}|$, and the fractional lipid charge, σ (identical with average number of charges per lipid molecule). Data are derived from lipid mixtures showing bilayer formation of case 1 as presented in Fig. 6 in the presence of EDTA (*open circles*) and calcium (*filled circles*), respectively. (*B*) Graph showing the time needed for bilayer formation, t_{SLB}, versus σ. Data are derived from lipid mixtures showing bilayer formation as presented in Fig. 6 in the presence of EDTA (*open circles*) and calcium (*filled circles*), respectively. t_{SLB} is determined from the onset of adsorption to equilibration of the signals in f and D. For DOPC/DOPS (molar ratio 1:1 and 1:2), extrapolated estimates are given.

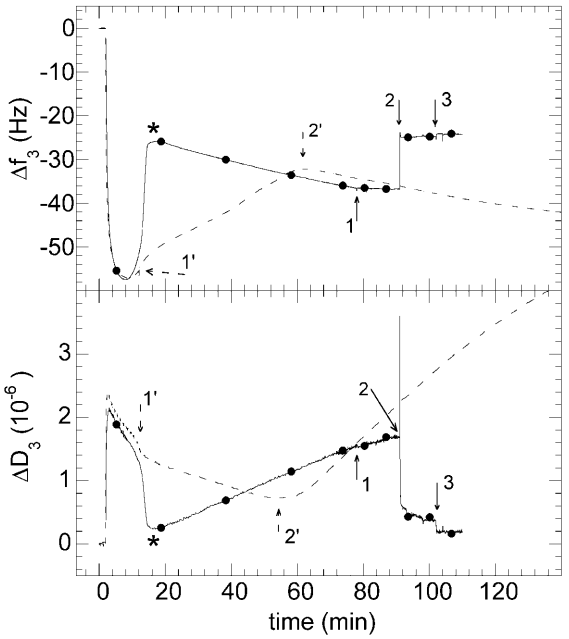

FIGURE 8 Restructuration of the adsorbed material into a more flexible conformational state after the onset of bilayer formation. QCM-D response for the adsorption of DOPC/DOPS (molar ratio 1:1) to SiO_2 in the presence of 2 mM $CaCl_2$. Changes in frequency (*upper panel*) and dissipation (*lower panel*) are given for two experiments, i), continuous line with closed circles, and ii), dashed line. In i), lipids present in solution were washed away ~65 min after the onset of restructuration (*asterisk*) by rinsing with calcium-containing buffer (*arrow 1*). A subsequent rinse with EDTA (*arrow 2*) resulted in a collapse of the flexible adlayer. The final values of Δf and ΔD after re-exposure to calcium (*arrow 3*) confirmed the formation of a complete SLB. In ii), removal of lipids present in solution was performed before the onset of restructuration by rinsing with calcium-containing buffer (*arrow 1′*). A decrease in f and an increase in D (*arrow 2′*) confirmed restructuration of surface-bound material in the absence of vesicles in solution.

decomposition (cf. Fig. 1 *B*). However, f subsequently decreased and D increased slowly (*arrow 2′* in Fig. 8). Since no extra lipid material was present in solution, these changes must correspond to a change of conformation or restructuration of the material adsorbed on the silica surface. The changes observed in f and D indicate that the restructured material was highly flexible and that additional water was associated with it.

DISCUSSION

In this study, we combined QCM-D and AFM methods to investigate the deposition of lipid vesicles of different net composition on silica surfaces. The main results are schematically described in Fig. 9. Three different pathways of vesicle deposition are distinguished: i), formation of a vesicular layer (scheme *C*), ii), formation of an SLB where vesicle decomposition occurs either at a high surface coverage (scheme *B*), and iii), at low surface coverage (scheme *A*). A fourth scenario corresponds with the absence of vesicle adsorption (scheme *D*).

Our results show that, for the lipid systems presented here, the net charge of the vesicles is the determining parameter for the type of pathway of vesicle decomposition.

Influence of the lipid charge on the vesicle deposition pathway

The processes of lipid vesicle deposition and SLB formation are governed by many types of interactions, as already extensively investigated experimentally and theoretically (Lipowsky and Seifert, 1991; Israelachvili, 1992; Seifert, 1997; Cremer and Boxer, 1999; Reviakine and Brisson, 2000; Zhdanov et al., 2000; Zhdanov and Kasemo, 2001; Reimhult et al., 2002a): i), the interaction between lipid vesicles and the support, ii), the interaction between adsorbed vesicles, and iii), the molecular interactions within adsorbed

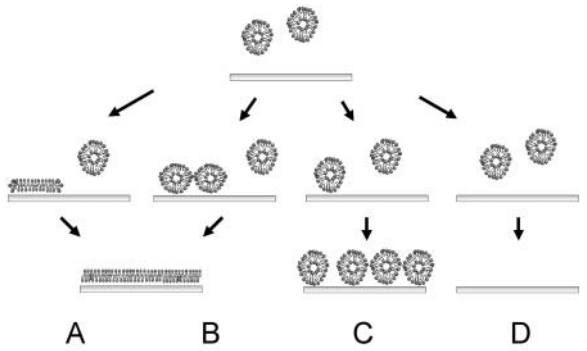

FIGURE 9 Schematic presentation of the pathways of vesicle deposition and SLB formation described in the text. (*A*) Formation of an SLB triggered at low vesicular coverage. (*B*) Formation of an SLB triggered at high vesicular coverage. (*C*) Formation of an SVL. (*D*) Inhibited adsorption.

vesicles, characterized by the bending modulus. It is logical to consider that electrostatic forces contribute to these three interactions, although a detailed description of their role as compared with other interactions such as that of van der Waals and steric interactions (Israelachvili, 1992) remains to be elucidated. Phenomenologically, a vesicle will rupture if the deformation that results from the three types of interactions exceeds a given threshold value. We will consider briefly our results according to this basic framework.

The fact that DOTAP SUVs, which are positively charged, rupture individually on negatively charged silica supports (Ducker et al., 1992; Arai et al., 1996) must reflect a strong vesicle-support electrostatic interaction, and possibly a reduced stability of isolated vesicles. On the other hand, the slow late stage of bilayer formation could result from an electrostatic repulsion between adsorbed DOTAP patches and SUVs in solution.

Vesicles with low positive (DOPC/DOTAP (4:1)), neutral (DOPC), or negative charge (DOPC/DOPS (4:1, 2:1)) adsorb but are not sufficiently deformed to auto-decompose. To induce decomposition, additional stress has to be provided by cooperative action of neighboring vesicles, i.e., a critical vesicular coverage is needed for bilayer formation (Keller et al., 2000; Reviakine and Brisson, 2000; Zhdanov et al., 2000). The fact that vesicle decomposition does not occur upon rinsing before the minimum frequency indicates that decomposition starts at or $\sim\Delta f_{min}$ and justifies using $|\Delta f_{min}|$ as a measure for the critical coverage. The increase of the critical coverage with decreasing vesicle charge (Fig. 7 *A*) is likely to reflect the fact that the interaction between vesicle and support is becoming less attractive as its electrostatic component diminishes, vanishes, or becomes repulsive for low positive, neutral, or negative vesicle charge, respectively. Interestingly, the dependence between $|\Delta f_{min}|$ and the fractional lipid charge, σ, is linear (Fig. 7 *A*), which deserves further investigation.

For vesicles with high net negative charge (DOPC/DOPS (1:1)), a stable SVL is obtained, indicating that, due to the combination of decreased vesicle-support interaction and increased intervesicle repulsion, vesicle decomposition cannot be initiated even at the highest attainable coverage. This adsorption barrier is responsible for the decreased initial adsorption rates observed for vesicles with a high net negative charge (DOPC/DOPS (2:1, 1:1)) and, eventually, the inhibition of adsorption for the highest negative charge employed (DOPC/DOPS (1:2)).

Effect of calcium

Calcium has already been reported to play an essential role in the process of bilayer formation, even at millimolar concentrations (McLaughlin et al., 1978; Gregory and Ginsberg, 1984; Feigenson, 1989; Leckband et al., 1993; Nollert et al., 1995; Reviakine et al., 2000). Our results confirm that calcium shifts the ability of bilayer formation toward higher negative vesicle charge. It is likely that this is due to the ability of the bivalent ion to ''bridge'' negatively charged entities such as the carboxylate groups in DOPS, the phosphate groups in DOPC and DOPS, or negative charges on the silica surface. In particular, the increase of the initial adsorption rates in the presence of calcium for DOPC/DOPS mixtures of composition ratio 2:1 and lower indicates the increased interaction between lipids and support.

Lateral organization

AFM provides local structural information on the formation of SLBs and further supports the interpretation of the QCM-D signal. The visualization of single vesicles, as well as patches of supported bilayers, gives insight into the structural changes of the surface-bound lipid material.

The case of DOPC/DOPS (4:1) is a typical example of bilayer formation induced at an elevated critical vesicular coverage. The use of the AFM tip as nanotweezers to induce the rupture of single vesicles allowed following the decomposition of neighboring vesicles into a bilayer patch. The obtained images suggest that supported bilayer domains grow by interaction of their active edges with adjacent vesicles. The visualization, in subsequent scan lines, of intermediate states of the bilayer domain growth (Fig. 3) allows estimating the propagation time to be in the order of 1 s. Domain growth stops as soon as a gap between the bilayer patch and neighboring vesicles is present. As supported vesicles and bilayer patches do not diffuse (at the timescale of minutes), the growth of SLBs in the absence of vesicles in solution is slow or eventually halts. The contribution of additional vesicles from solution is required to initiate new cascades of vesicle rupture events. This process, combined with formation of new bilayer patches, continues until eventually the whole surface is covered (Reviakine and Brisson, 2000; Zhdanov et al., 2000).

In the case of the DOPC/DOPS (4:1) mixture, our results indicate that bilayer formation does not involve fusion of surface-bound vesicles because i), the size distribution of surface-bound vesicles did not change dramatically with increasing surface coverage, and ii), no indications of fusion intermediates could be found when inducing the formation of bilayer patches by the AFM tip (Fig. 3).

For both SLB-formation pathways, stable bilayer patches of noncircular shape have been observed. This indicates support-induced constraints on the lipid mobility, as a non-constrained patch would adopt the thermodynamically favorable circular shape (Muresan and Lee, 2001). It is unclear, though, whether the mobility constraints are prevalent in the entire support-facing monolayer or only on its edges.

We suggest that the large size distribution of bilayer patches, observed for DOTAP at low coverage, originates from a large size distribution of vesicles present in solution. The formation of DOTAP-SUVs by sonication might be more difficult due to the elevated charge density, as compared with DOPC. It is considered less likely that the bilayer patches are the result of the fusion of several small vesicles on the surface since this should result in more homogeneous surface coverage than observed.

Even though the overall results obtained by AFM and QCM-D confirmed each other, it should be underlined that the supports used for AFM and QCM-D were not identical. Notably, the fact that SLB formation with DOTAP was found to be complete on silica wafers by AFM, whereas some uncovered support was detected by QCM-D, could be due to varying surface roughness or slightly different chemical properties of the support. Also, a detailed analysis of adsorbed lipid material in terms of surface coverage was not attempted here because of difficulties to independently extract accurate values from AFM and QCM-D data.

Restructuration

For a number of lipid compositions, a restructuration of surface-bound lipid material into a more flexible state upon association of water was observed to set in before the SLB formation was finished. This underlines that SLB formation is largely dependent on the lipid composition, and that the exposure of vesicles to a solid support can lead to more diverse structures than SVLs and SLBs.

Restructuration was characterized by kinetics significantly slower than the bilayer formation. Calcium plays an important role in this process, as it was never observed in EDTA and as the flexible structure collapses within seconds after exposure to EDTA. It remains to be elucidated which parts of the surface-bound lipid material—vesicles or bilayer patches—participate in the restructuration, and what is the mesoscopic structure of the flexible adlayer. However, since restructuration is not reinduced by adding Ca^{2+} ions or vesicles on a continuous bilayer formed by collapse with EDTA (Fig. 8), we tentatively propose that restructuration is triggered by active bilayer edges.

The influence of electrostatic interaction in general and the lipid charge in particular on vesicle deposition and SLB formation has frequently been reported (Nollert et al., 1995; Cremer and Boxer, 1999; Egawa and Furusawa, 1999). We could demonstrate that the variation of the lipid charge only can lead to several different vesicle deposition pathways. Notably, the pathway of bilayer formation induced at low vesicular coverage could be observed for the first time by QCM-D, which allowed a direct comparison of the two pathways of bilayer formation reported. The charge changes the balance between vesicle-support, intervesicle, and intra-bilayer interactions and is thus a determinant of the vesicle deposition pathway.

It is understood that the two pathways of SLB formation established here are not exclusive. Other pathways are possible, including an intermediate step of fusion of surface-bound vesicles, as observed for small vesicles of egg-PC on mica (Reviakine and Brisson, 2000). The three types of interactions (bilayer-support, interbilayer, and intrabilayer) might also influence the molecular interaction of lipids in a bilayer, e.g., leading to segregation (Reviakine et al., 2000) or changes in the bilayer fluidity, and thus indirectly change the stability of adsorbed vesicles and the vesicle decomposition pathway.

The results obtained by AFM confirm the interpretation of QCM-D data on SLB formation presented here as well as by Kasemo and co-workers (Keller and Kasemo, 1998; Keller et al., 2000; Reimhult et al., 2003). The study emphasizes the complementarity between QCM-D, which is a quick and straightforward method and enables screening for relevant experimental conditions, and AFM, which allows detailed structural investigation, yet is more laborious for soft samples.

It can be anticipated that the combination of these techniques as well as other techniques such as fluorescence microscopy (Boxer, 2000; Johnson et al., 2002; Kiessling and Tamm, 2003) or spectroscopy (Watts et al., 1986), surface plasmon resonance (Keller et al., 2000), and ellipsometry (Benes et al., 2002) will help to improve the description of the SLB-formation pathways. Important questions to be answered are the exact role of vesicles in solution in the late stage of the SLB-formation process, the influence of lateral diffusion of adsorbed vesicles/bilayer patches, the role of fusion intermediates, the orientation of the lipid layers after vesicle rupture, the critical vesicular coverage preceding SLB formation, and the possible loss of surface-bound lipid material.

CONCLUSION

This report demonstrates that the variation of the charge of lipid vesicles allowed tuning the pathway of bilayer formation. It was established that several pathways of vesicle deposition and bilayer formation are possible. The

lipid charge changes the balance between vesicle-support, intervesicle, and intrabilayer interactions, thus becoming a determinant of the vesicle-deposition pathway. Calcium was shown to enhance the tendency of bilayer formation.

The basic techniques employed, AFM and QCM-D, were shown to be highly complementary for this study, providing an effective characterization of both the overall dynamics and a spatially resolved picture of the lipid deposition process. The ability to predict and control the formation of SLBs is a potentially important step toward designing biofunctional surfaces.

Discussions with Fredrik Höök (Q-Sense), Erik Reimhult (Chalmers, Gothenburg, Sweden), and Olivier Lambert (Institut Europen de Chimie et Biologie) are acknowledged. We thank Patrice Caillat and Claude Vauchier (Commissariat à l'Energie Atomique-Laboratoire d'Electronique de Technologie de l'Information, Grenoble, France) for the gift of silicon wafers.

R.R. is the recipient of a PhD fellowship from the Conseil Régional d'Aquitaine, France. This research was supported by the Conseil Régional d'Aquitaine, the Fonds Européen de Développement Régional, and European Commission grants QLK2-CT2001-01339 and QLG3-CT2001-00902.

REFERENCES

Adamczyk, Z., B. Siwek, M. Zembala, and P. Belouschek. 1994. Kinetics of localized adsorption of colloid particles. *Adv. Colloid Int. Sci.* 48:151–280.

Arai, T., D. Aoki, Y. Okabe, and M. Fujihira. 1996. Analysis of surface forces on oxides in aqueous solutions using AFM. *Thin Solid Films.* 273:322–326.

Benes, M., D. Billy, W. T. Hermens, and M. Hof. 2002. Muscovite (mica) allows the characterisation of supported bilayers by ellipsometry and confocal fluorescence correlation spectroscopy. *Biol. Chem.* 383:337–341.

Bieri, C., O. P. Ernst, S. Heyse, K. P. Hofmann, and H. Vogel. 1999. Micropatterned immobilization of a G protein-coupled receptor and direct detection of G protein activation. *Nat. Biotechnol.* 17:1105–1108.

Boxer, S. G. 2000. Molecular transport and organization in supported lipid membranes. *Curr. Opin. Chem. Biol.* 4:704–709.

Cornell, B. A., V. L. Braach-Maksvytis, L. G. King, P. D. Osman, B. Raguse, L. Wieczorek, and R. J. Pace. 1997. A biosensor that uses ion-channel switches. *Nature.* 387:580–583.

Cremer, P. S., and S. G. Boxer. 1999. Formation and spreading of lipid bilayers on planar glass supports. *J. Phys. Chem. B.* 103:2554–2559.

Ducker, W. A., T. J. Senden, and R. M. Pashley. 1992. Measurement of forces in liquids using a force microscope. *Langmuir.* 8:1831–1836.

Egawa, H., and K. Furusawa. 1999. Liposome adhesion on mica surface studied by atomic force microscopy. *Langmuir.* 15:1660–1666.

Ekeroth, J., P. Konradsson, and F. Höök. 2002. Bivalent-ion-mediated vesicle adsorption and controlled supported phospholipid bilayer formation on molecular phosphate and sulfate layers on gold. *Langmuir.* 18:7923–7929.

Feigenson, G. W. 1989. Calcium ion binding between lipid bilayers: the four-component system of phosphatidylserine, phosphatidylcholine, calcium chloride, and water. *Biochemistry.* 28:1270–1278.

Gregory, D. P., and L. Ginsberg. 1984. Calcium association with phosphatidylserine: modification by cholesterol and phosphatidylcholine in monolayers and bilayers. *Biochim. Biophs. Acta.* 769:238–244.

Israelachvili, J. N. 1992. Intermolecular and Surface Forces. Academic Press, London.

Jass, J., T. Tjärnhage, and G. Puu. 2000. From liposomes to supported, planar bilayer structures on hydrophilic and hydrophobic surfaces: an atomic force microscopy study. *Biophys. J.* 79:3153–3163.

Johnson, J. M., H. Taekijp, S. Chu, and S. G. Boxer. 2002. Early steps of supported bilayer formation probed by single vesicle fluorescence assays. *Biophys. J.* 83:3371–3379.

Keller, C. A., K. Glasmästar, V. P. Zhdanov, and B. Kasemo. 2000. Formation of supported membranes from vesicles. *Phys. Rev. Lett.* 84:5443–5446.

Keller, C. A., and B. Kasemo. 1998. Surface specific kinetics of lipid vesicle adsorption measured with a quartz crystal microbalance. *Biophys. J.* 75:1397–1402.

Kiessling, V., and L. K. Tamm. 2003. Measuring distances in supported bilayers by fluorescence interference-contrast microscopy: polymer supports and SNARE proteins. *Biophys. J.* 84:408–418.

Kung, L. A., L. Kam, J. S. Hovis, and S. G. Boxer. 2000. Patterning hybrid surfaces of proteins and supported lipid bilayers. *Langmuir.* 16:6773–6776.

Leckband, D. E., C. A. Helm, and J. Israelachvili. 1993. Role of calcium in the adhesion and fusion of bilayers. *Biochemistry.* 32:1127–1140.

Liebau, M., A. Hildebrand, and R. H. Neubert. 2001. Bioadhesion of supramolecular structures at supported planar bilayers as studied by the quartz crystal microbalance. *Eur. Biophys. J.* 30:42–52.

Lipowsky, R., and U. Seifert. 1991. Adhesion of vesicles and membranes. *Mol. Crys. Liq. Cryst.* 202:17–25.

Marcelja, S. 1992. Electrostatics of membrane adhesion. *Biophys. J.* 61:1117–1121.

McConnell, H. M., T. H. Watts, R. M. Weis, and A. A. Brian. 1986. Supported planar membranes in studies of cell-cell recognition in the immune system. *Biochim. Biophys. Acta.* 864:95–106.

McLaughlin, A., C. Grathwohl, and S. McLaughlin. 1978. The adsorption of divalent cations to phosphatidylcholine bilayer membranes. *Biochim. Biophys. Acta.* 513:338–357.

Muresan, A. S., and K. Y. C. Lee. 2001. Shape evolution of lipid bilayer patches adsorbed on mica: an atomic force microscopy study. *J. Phys. Chem. B.* 105:852–855.

Nollert, P., H. Kiefer, and F. Jähnig. 1995. Lipid vesicle adsorption versus formation of planar bilayers on solid surfaces. *Biophys. J.* 69:1447–1455.

Pignataro, B., C. Steinem, H.-J. Galla, H. Fuchs, and A. Janshoff. 2000. Specific adhesion of vesicles monitored by scanning force microscopy and quartz crystal microbalance. *Biophys. J.* 78:487–498.

Reimhult, E., F. Höök, and B. Kasemo. 2002a. Temperature dependence of formation of a supported phospholipid bilayer from vesicles on SiO_2. *Phys. Rev. E.* 66:051905.

Reimhult, E., F. Höök, and B. Kasemo. 2002b. Vesicle adsorption on SiO_2 and TiO_2: dependence on vesicle size. *J. Chem. Phys.* 117:7401–7404.

Reimhult, E., F. Höök, and B. Kasemo. 2003. Intact vesicle adsorption and supported biomembrane formation from vesicles in solution: influence of surface chemistry, vesicle size, temperature and osmotic pressure. *Langmuir.* In press.

Reviakine, I., W. Bergsma-Schutter, and A. Brisson. 1998. Growth of protein 2-D crystals on supported planar lipid bilayers imaged in situ by AFM. *J. Struct. Biol.* 121:356–361.

Reviakine, I., and A. Brisson. 2000. Formation of supported phospholipid bilayers from unilamellar vesicles investigated by atomic force microscopy. *Langmuir.* 16:1806–1815.

Reviakine, I., A. Simon, and A. Brisson. 2000. Effect of Ca^{2+} on the morphology of mixed DPPC-DOPS supported phospholipid bilayers. *Langmuir.* 16:1473–1477.

Richter, R., and A. Brisson. 2003. Characterization of lipid bilayers and protein assemblies supported on rough surfaces by atomic force microscopy. *Langmuir.* In press.

Rodahl, M., F. Höök, A. Krozer, P. Brzezinski, and B. Kasemo. 1995. Quartz crystal microbalance setup for frequency and Q-factor measurements in gaseous and liquid environments. *Rev. Sci. Instrum.* 66:3924–3930.

Rouser, G., S. Fleisher, and A. Yamamoto. 1975. Two-dimensional thin layer chromatographic separation of polar lipids and determination of phospholipids by phosphorus analysis of spots. *Lipids*. 5:494–496.

Rädler, J., H. Strey, and E. Sackmann. 1995. Phenomenology and kinetics of lipid bilayer spreading on hydrophilic surfaces. *Langmuir*. 11:4539–4548.

Sackmann, E. 1996. Supported membranes: scientific and practical applications. *Science*. 271:43–48.

Salafsky, J., J. T. Groves, and S. G. Boxer. 1996. Architecture and function of membrane proteins in planar supported bilayers: a study with photosynthetic reaction centers. *Biochemistry*. 35:14773–14781.

Seifert, U. 1997. Configuration of fluid membranes and vesicles. *Adv. Phys*. 46:13–137.

Watts, T. H., A. A. Brian, J. W. Kappler, P. Marrack, and H. M. McConnell. 1984. Antigen presentation by supported planar membranes containing affinity-purified I-Ad. *Proc. Natl. Acad. Sci. USA*. 81:7564–7568.

Watts, T. H., H. E. Gaub, and H. M. McConnell. 1986. T-cell-mediated association of peptide antigen and major histocompatibility complex protein detected by energy transfer in an evanescent wave-field. *Nature*. 320:179–181.

Vig, J. R. 1987. UV/ozone cleaning of surfaces. *In* Treatise on Clean Surface Technology. K. L. Mittal, editor. Plenum Press, New York. 1–26.

Wilschut, J., N. Düzgünes, and D. Papahadjopoulos. 1981. Calcium/magnesium specificity in membrane fusion: kinetics of aggregation and fusion of phophatidylserine vesicles and the role of bilayer curvature. *Biochemistry*. 20:3126–3133.

Zhdanov, V. P., and B. Kasemo. 2001. Comments on rupture of adsorbed vesicles. *Langmuir*. 17:3518–3521.

Zhdanov, V. P., C. A. Keller, K. Glasmästar, and B. Kasemo. 2000. Simulation of adsorption kinetics of lipid vesicles. *J. Chem. Phys*. 112:900–909.